Using Structural Degradation and Parallax for Reduced-reference Quality Assessment of 3D Images

Qi Xu, Guangtao Zhai, Min Liu and Ke Gu
Institute of Image Communication and Information Processing, Shanghai Jiao Tong University
Shanghai Key Laboratory of Digital Media Processing and Transmissions
Shanghai, China
Email: xuqi@sjtu.edu.cn

***Abstract*—Owing to the thriving market of stereoscopic image based applications, efficient and effective 3D image quality assessment (IQA) techniques become colossally required these days. Consequently, we introduce a new reduced-reference (RR) stereoscopic image quality metric to meet this demand, through measuring Structural degradation and Saliency based Parallax compensation Model (SSPM). Experimental results on the LIVE 3D Image Quality Database, including both symmetrically and asymmetrically distorted stereoscopic images in different categories and quality levels, are provided to justify the effectiveness of the proposed SSPM model as compared to some existing progressive and popular stereoscopic IQA approaches. Meanwhile, it deserves broad attentions that only four number pairs, extracted from original image, are required as the key feature to be sent to the receiver terminal, thus making this procedure also efficient.**

***Keywords*—Performance evaluation, objective evaluation techniques, image quality assessment (IQA), stereoscopic image, reduced-reference (RR), structural degradation, parallax compensation, saliency**

I. Introduction

In these years, human beings gradually incline to pursuing multimedia contents with higher quality in the traditional entertainment areas such as motion pictures and video games, as well as some more specialized fields, including education and medicine. For this reason, image quality assessment (IQA) has drawn numerous interests from researchers in these fields. During the last decade, besides the classical peak signal-to-noise ratio (PSNR), many impressive objective 2D IQA approaches have been developed, including human visual system (HVS) inspired structural similarity index (SSIM) [1], multi-scale SSIM (MS-SSIM) [2], visual information fidelity (VIF) [3], and etc. These remarkable 2D image quality metrics are all well correlated to the subjective mean opinion score (MOS), and therefore contribute adequate models and theoretical supports.

Indeed, researchers nowadays tend to show increasing interest in IQA for stereoscopic images to meet the demand of the wide application with 3D imaging techniques. In general, most 3D imagining techniques are to separately present two 2D image in slight difference to the left and the right eye, and then the 3D image is established in the brain with the certain perception of 3D depth, which means that a stereoscopic image is in fact some combination of two 2D images. Therefore, it is naturally occurred to researchers in the field that 2D IQA approaches should feasibly be extended to handle stereoscopic images.

Actually about five years ago, an early full-reference (FR) stereoscopic IQA method [4] was developed based on the fusion of 2D quality metrics and the depth information. Subsequently, another FR stereoscopic quality metric [5] discussed different integrations of existing 2D IQA methods and disparity information. In the same year, [6] proposed a reduced-reference (RR) stereoscopic IQA approach using edges and contours of 3D depth map as the extracted information. Recently, no-reference 3D IQA methods [7]-[8] are exploited for 3D JPEG compressed images, by means of combining 2D quality metric [9] and parallax compensation. Accordingly, we have a good reason to believe that extending 2D image quality metric, combined with stereoscopic information between left and right images, is a desirable and promising direction.

From the viewpoint of simulating the behaviour of the HVS, researches on stereoscopic IQA indicate that 2D quality metric adding stereoscopic information of the 3D image pairs is not just a practical product, but also theoretically advocated by a finding [10]. This discovery depicts that cells in the retina of each eye individually encode their received visual signal, and then the coded information, later merged in lateral geniculate nucleus (LGN), formulate the ultimate stereoscopic image in the brain. Following this line of research, we consequently propose a new RR stereoscopic IQA approach by means of combining two basic parts. One of them is the recently proposed structural degradation model (SDM) [11] for RR image quality assessment. This 2D IQA approach is mainly developed based on an interesting observation mentioned in a previous work [12] that pre-processed by low-pass filtering, images with various distortion categories and quality levels will have different degrees of spatial frequency decrease. And the other part adopts saliency based parallax compensation method to measure the uncomfortable feeling under the condition of high degree of parallax.

The remainder of this paper is arranged as the following. Section II foremost presents the definition and description of the feature extraction and the saliency based parallax compensation, and then the Structural degradation and Saliency based Parallax compensation Model (SSPM) is introduced. In Section III, the performance of our model is reported and analyzed on the recently released LIVE 3D Image Quality Database Phase 1 [13] and Phase 2 [17], [18], which contain several 3D images, as well as their symmetrically and asymmetrically distorted versions in different categories and various quality levels. Finally, concluding remarks are given in Section IV.

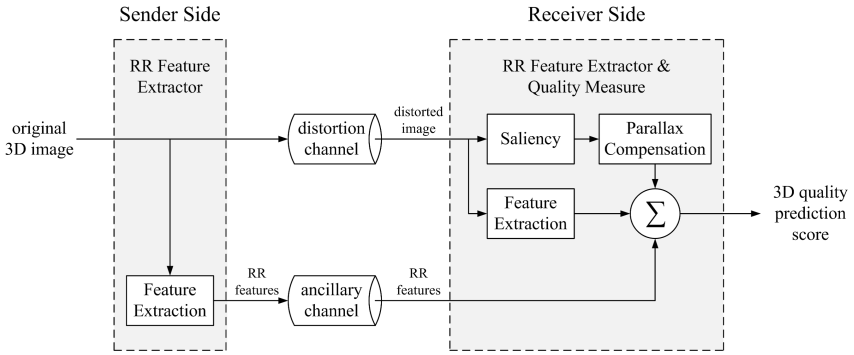

Fig. 1. The flowchart of the proposed SSPM model based RR stereoscopic IQA approach. It shows that the quality of a distorted 3D image can be estimated by a carefully designed nonlinear combination of the certain extracted features of this distorted stimulus and the original version of it, with the saliency based parallax compensation of it.

II. The Prediction Model

Our proposed reduced-reference 3D IQA metric (SSPM) can be executed according to the flowchart in Fig. 1. It is not difficult to acquire that there are three cardinal steps included for measuring SSPM, which are feature extraction, saliency based parallax compensation, and an effective nonlinear combination. As the demonstration in Fig. 1, we foremost adopt the recently proposed structural degradation information [12] in the sender side. In spite of the fact that the structural degradation information is originated from structural information [1], it has more flexibility in assessing image quality, because the structural degradation information can flourishingly discriminates disparate distortion types, as mentioned in [12]. In this work, the structural degradation information for the original left or right image is defined as

$$\begin{aligned} SD_{m,t}(X_L) &= SSIM(\mu_{X_{(L)}}(d=0.1), \mu_{X_{(L)}}(d=1.5)) \\ SD_{v,t}(X_L) &= SSIM(\sigma_{X_{(L)}}(d=0.1), \sigma_{X_{(L)}}(d=1.5)) \end{aligned} \quad (1)$$

$$\begin{aligned} SD_{m,t}(X_R) &= SSIM(\mu_{X_{(R)}}(d=0.1), \mu_{X_{(R)}}(d=1.5)) \\ SD_{v,t}(X_R) &= SSIM(\sigma_{X_{(R)}}(d=0.1), \sigma_{X_{(R)}}(d=1.5)) \end{aligned} \quad (2)$$

where X_L/X_R represents the original left/right image, while *m* and *v* correspond to $\mu_{X_{(L)}}(d)$ and $\sigma_{X_{(L)}}(d)$ (or $\mu_{X_{(R)}}(d)$ and $\sigma_{X_{(R)}}(d)$). In addition, $t = \{i, e\}$ is for interior parts or exterior parts of blocks. As illustrated in Fig. 2, for a block with the size of 8×8, the dark gray part is the exterior part, while the middle part colored with light gray is the interior part. Moreover, the function *SSIM(·)* is defined in a previous work [1].

Referring to the initial definitions of μ_X and σ_X in [1], we reconfigure $\mu_{X_{(L)}}(d)$ and $\sigma_{X_{(L)}}(d)$ (or $\mu_{X_{(R)}}(d)$ and $\sigma_{X_{(R)}}(d)$) as:

$$\begin{aligned} \mu_{X_{(L)}}(d) &= \frac{1}{N^2}\sum_{i=1}^{N}\sum_{j=1}^{N} w_{ij} x_{(L)_{ij}} \\ \sigma_{X_{(L)}}(d) &= \frac{1}{N^2-1}\sum_{i=1}^{N}\sum_{j=1}^{N} w_{ij}(x_{(L)_{ij}} - \mu_{X_{(L)}}(d))^2 \end{aligned} \quad (3)$$

$$\begin{aligned} \mu_{X_{(R)}}(d) &= \frac{1}{N^2}\sum_{i=1}^{N}\sum_{j=1}^{N} w_{ij} x_{(R)_{ij}} \\ \sigma_{X_{(R)}}(d) &= \frac{1}{N^2-1}\sum_{i=1}^{N}\sum_{j=1}^{N} w_{ij}(x_{(R)_{ij}} - \mu_{X_{(R)}}(d))^2 \end{aligned} \quad (4)$$

with $w = \{w_{ij} | i, j = 1, ..., N\}$, satisfying $Sum(w) = 1$ and $Var(w) = d$ (function $Sum(\cdot)$ and $Var(\cdot)$) are used to compute the sum and variance values, respectively).

While the distorted stereoscopic image is sent to the receiver side through the distortion channel, four number pairs ($SD_{m,t}(X_L)$, $SD_{v,t}(X_L)$, $SD_{m,t}(X_R)$ and $SD_{v,t}(X_R)$, with $t = \{i, e\}$) are extracted as the RR features and transferred to the reviewer side. Afterward, the feature extraction procedure is compulsory in the stage of the receiver as well. In this case, the structural degradation information of distorted 3D image Y ($SD_{m,t}(Y_L)$, $SD_{v,t}(Y_L)$, $SD_{m,t}(Y_R)$ and $SD_{v,t}(Y_R)$, with $t = \{i, e\}$) are correspondingly evaluated in accordance with the method for computing that of the original image X.

Compared to 2D image quality metrics, besides the image pair themselves, stereoscopic IQA dramatically depends on stereoscopic information between the left and right images as well. In general, it is probably admitted that the higher qualities of left and right images are, the higher quality of the corresponding 3D image will be. In this work, we find this common sense, however, is not always valid. To justify, an experiment has been conducted by taking advantage of two indicating original stereoscopic images that are carefully selected

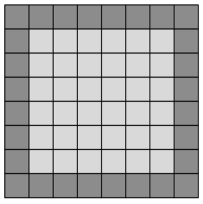

Fig. 2. An illustration of interior parts or exterior parts of blocks. For a block with the size of 8×8, the dark gray part is the exterior part, while the middle part colored with light gray is the interior part.

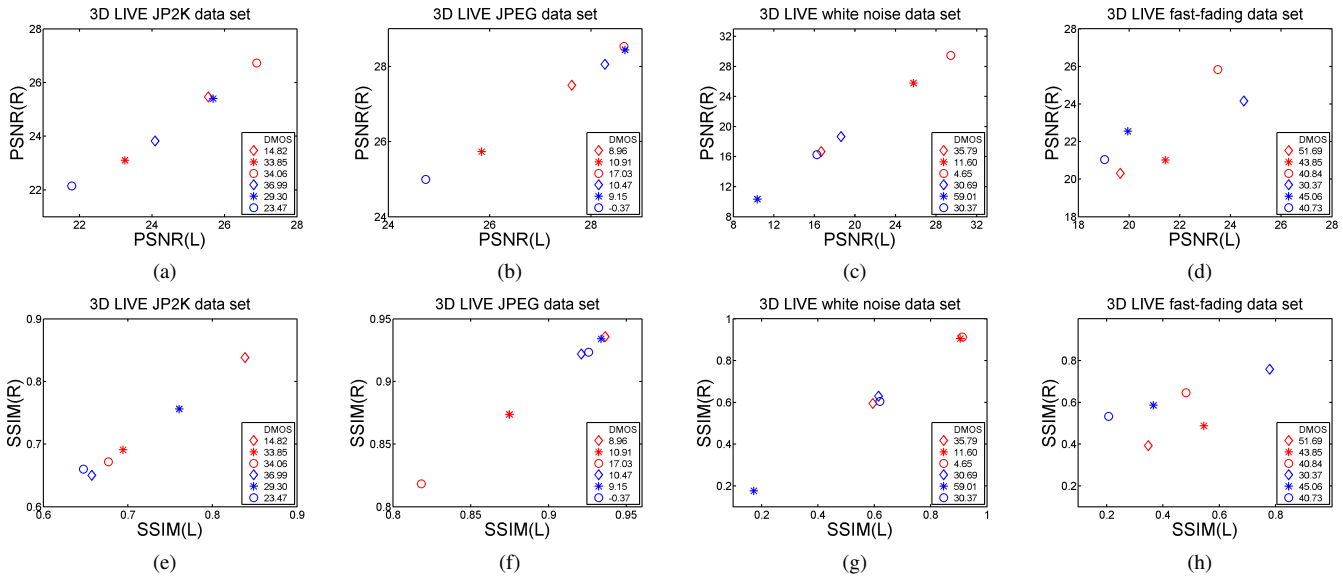

Fig. 3. The illustration of the relationship between DMOS value of a stereoscopic image and the corresponding PSNR (or SSIM) results of left and right images. Red symbols indicate distorted 3D images corresponding to the original 3D image of Fig. 4 (a) and (b), while blue symbols are the contaminated versions of Fig. 4 (c) and (d). Note that the lower DMOS of an image indicates its higher image quality.

from the LIVE 3D Image Quality Database Phase 1 [13], as illustrated in Fig. 4. Their distorted stimuli are subjected to JPEG2000 and JPEG compression, white noise injection and fast-fading. Since these two pair of typical samples are chosen from the Phase 1 database, the corresponding left and right images are distorted symmetrically.

In this case, we apply two of the most classical IQA approaches, PSNR and SSIM, to evaluate the qualities of these four pictures, noted as PSNR(Y_L), PSNR(Y_R), SSIM(Y_L) and SSIM(Y_R). Fig. 3 displays the relationship between 3D image qualities and the corresponding couples of PSNR(Y_L) and PSNR(Y_R) (or SSIM(Y_L) and SSIM(Y_R)) values. Red symbols indicate distorted versions of the original 3D image pair Fig. 4 (a) and (b), while blue symbols are the contaminated versions of Fig. 4 (c) and (d). In addition, DMOS of each sample is also presented in the label of figures in Fig. 3 and several fascinating phenomena are recognized. Contrast to the common sense, higher left/right image qualities do not necessarily lead to higher 3D quality indeed. As far as Fig. 3 (a), (b) and (e) are concerned, the blue "○", indicating 3D images with lower qualities of both 2D images, yet have a higher 3D image quality. Furthermore, Fig. 3 (d) shows that 3D images corresponding to red "○" and blue "◇" have close 2D image quality but different 3D qualities. On the other hand, the SSIM metric, however, is capable of eliminating the mentioned anomaly in some cases. In other words, the structural information should possibly have more positive effect on measuring stereoscopic image quality. For instance, it is obvious that the red and blue "○" corresponding to SSIM scores in Fig. 3 (f) manage to conquer the anomaly, while PSNR results in Fig. 3 (e) show an inferior performance. This discovery encourages us to adopt the formerly mentioned structural degradation information (the improved structural information) as an effective feature for the proposed RR IQA approach.

We believe that this anomaly is related to both image contents and stereoscopic parallax. Take the pictures in Fig. 4 for example once more, these two pairs have very similar scene, including a mountain bike, fence and a teaching building, yet with different saliency regions and degrees of parallax. Furthermore, it is observed in [14] that the low subjective evaluation is introduced from high degrees of parallax. We therefore attribute the above-mentioned anomaly to uneven parallax, and adopts an effective compensation technique following the underlying idea of [7]. The parallax is defined to reimburse the anomaly as follows with $|\cdot|_2$ being 2 order norm:

$$\rho = cos^{-1}(\frac{< Y_L \cdot Y_R >}{|Y_L|_2 \cdot |Y_R|_2}) \tag{5}$$

Inspired by the behavior and the neuronal architectures of the early primate visual system, a classic saliency model [15] has been developed to construct a single topographical saliency map. This model first combine multi-scale image features,

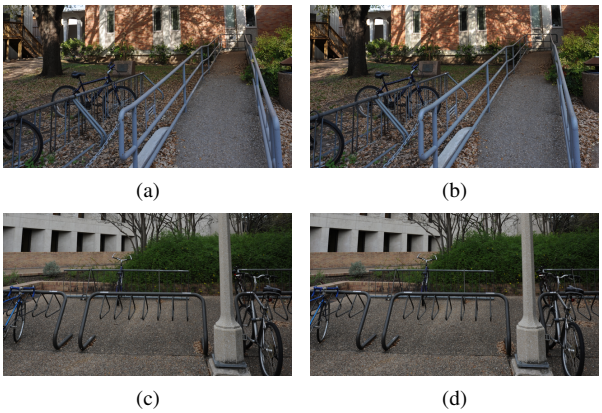

Fig. 4. The carefully selected two representative original stereoscopic images with similar scene but different saliency regions and degrees of parallax.

including colors, intensity and orientations, and then a winner-take-all network, which implements a neutrally distributed maximum detector, is performed to detect the most salient locations gradually until the final saliency map is achieved. To further explore Eq. (5) by employing this saliency model, the saliency based parallax can be evaluated as:

$$\rho_S = cos^{-1}(\frac{< Y_L(S) \cdot Y_R(S) >}{|Y_L(S)|_2 \cdot |Y_R(S)|_2}) \tag{6}$$

where S represents saliency regions computed by the authors of [15]. To compensate the uncomfortable parallax, the saliency based parallax compensation is ultimately estimated by:

$$P(Y) = w \cdot \rho + w_S \cdot \rho_S \tag{7}$$

with w and w_S being model parameters.

After feature extraction and saliency based parallax compensation parts are well illustrated in the receiver side, we still confront a major problem on combining the extracted features and the saliency based parallax compensation. Owing to the fact discovered in some previous works that the difference between structural degradation information of the original image X and distorted image Y can discriminate the five commonly seen distortion categories, we consequently define the distance of structural degradation information as:

$$D_{V,s,t} = SD_{s,t}(X_V) - SD_{s,t}(Y_V). \tag{8}$$

where $s = \{m, v\}$, $t = \{i, e\}$ and $V = \{L, R\}$.

Then, the $G(D_{V,s,t})$ is carefully defined to measure the image quality for one group of the given $\{V, s, t\}$ values. In this case, $G(D_{V,s,t})$ can be valued by:

$$G(D_{V,s,t}) = \lambda_{s,t} \cdot (D_{V,s,t})^{\gamma_{s,t}} \tag{9}$$

where $\lambda_{s,t}$ and $\gamma_{s,t}$, with $s = \{m, v\}$ and $t = \{i, e\}$, are the model parameters.

Finally, the proposed SSPM model is designed by properly combining $G(D_{V,s,t})$ and $P(Y)$. Following the format used in [4], our SSPM model is defined as:

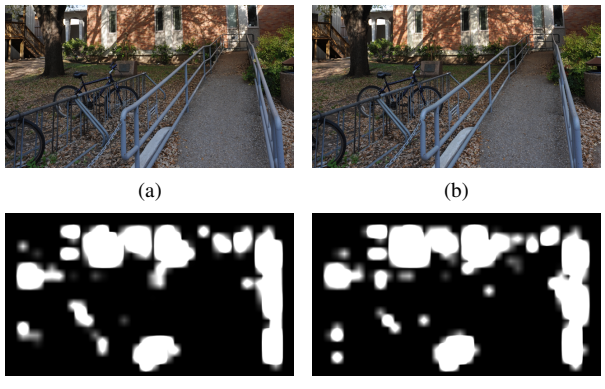

(a) (b) (c) (d)

Fig. 5. An example of a pair of stereoscopic image and its saliency map. The highlighted white regions in (c) and (d) are determined as the saliency regions of the scene shown in (a) and (b).

$$\begin{aligned} SSPM &= (2D\ qualities\ sum)(\frac{1}{2} + parallax\ value) \\ &= [\sum G(D_{V,s,t})] \cdot (\frac{1}{2} + P(Y)) \end{aligned} \tag{10}$$

where $s = \{m, v\}$, $t = \{i, e\}$ and $V = \{L, R\}$.

III. Experimental Results

Performance of SSPM metric is tested on the LIVE 3D Image Quality Database, which contains 2 phases and various distortion levels. Phase 1 [13] includes 20 reference 3D images and 365 symmetrically distorted stimuli of them, while Phase 2 [17], [18] contains 8 reference images and 360 distorted stimuli including both symmetrically and asymmetrically distorted versions. For comparison, mappings of the scores to subjective scores of our proposed SSPM together with mainstream metrics, including Benoit [4], You [5], Hewage [6], Chen [17], Cyclopean MS-SSIM [18] and Akhter [19], are obtained after using nonlinear regression with a logistic function suggested by VQEG [16]:

$$q(z) = \frac{\xi_1 - \xi_2}{1 + exp(-\frac{z - \xi_3}{\xi_4})} + \xi_2 \tag{11}$$

with z and $q(z)$ being the input score and the mapped score, respectively. The free parameters ξ_1 - ξ_4 are to be determined during the curve fitting process.

In order to further evaluate the competitive SSPM metrics, we apply three performance metrics for comparison, involving Pearson Linear Correlation Coefficient (PLCC), Spearman Rank-Order Correlation Coefficient (SROCC), and Root Mean-Squared Error (RMSE) as suggested by VQEG [16]. Note that Benoit [4], You [5] and Cyclopean MS-SSIM [18]are full-reference metrics, Chen [17] and Akhter [19] are no-reference methods, while Hewage [6] and our proposed SSPM are reduced-reference algorithms.

A. Performance on LIVE 3D Database Phase 1

Table I-III tabulate the performance results, and the scatter plots of differential MOS (DMOS) versus SSPM on the overall LIVE 3D database Phase 1 and five data sets of different distortion categories are shown in Fig. 6.

It is explicit that our paradigm has achieved much better results than the mainstream FR ,RR and NR stereoscopic IQA methods while images are distorted symmetrically, especially for JPEG compression.

TABLE I. SROCC values of the mainstream 3D IQA metrics on the LIVE 3D database Phase 1

Algorithm	WN	JP2K	JPEG	GBlur	FF	All
Benoit [4]	0.930	0.910	0.603	0.931	0.699	0.899
You [5]	0.940	0.860	0.439	0.882	0.588	0.878
C. MS-SSIM [18]	0.948	0.888	0.530	0.925	0.707	0.916
Hewage [6]	0.940	0.856	0.500	0.690	0.545	0.814
SSPM	0.920	0.843	0.701	0.857	0.691	0.916
Chen [17]	0.919	0.863	0.617	0.878	0.652	0.891
Akhter [19]	0.914	0.866	0.675	0.555	0.640	0.383

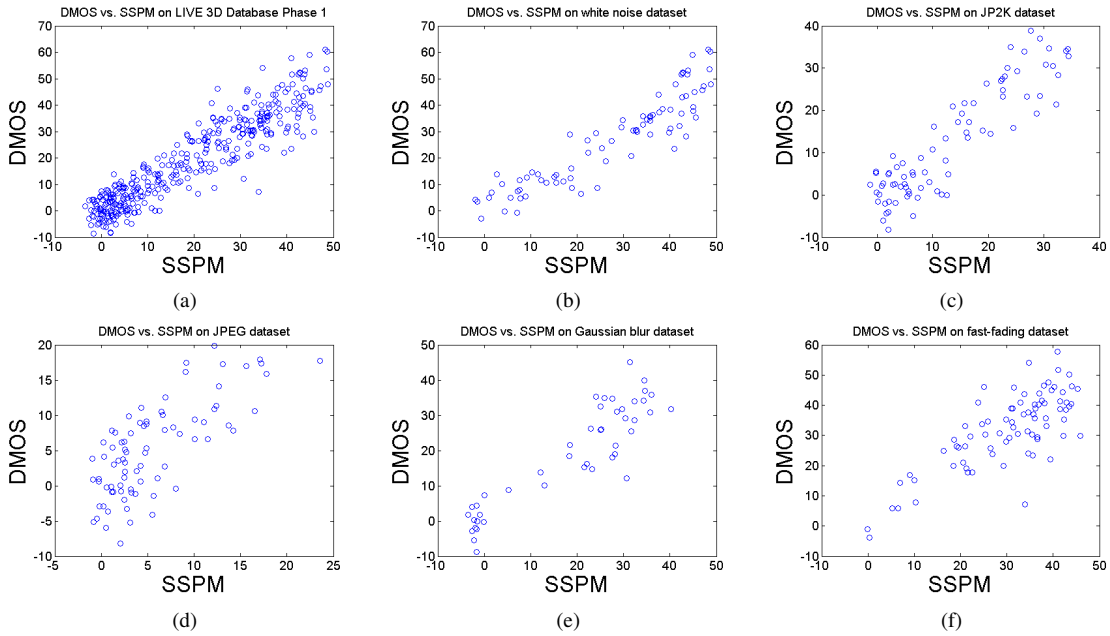

Fig. 6. Scatter plots of DMOS vs. the proposed SSPM metric on the whole LIVE 3D database Phase 1 and five data sets of different distortion types.

TABLE II. PLCC VALUES OF THE MAINSTREAM 3D IQA METRICS ON THE LIVE 3D DATABASE PHASE 1

Algorithm	WN	JP2K	JPEG	GBlur	FF	All
Benoit [4]	0.925	0.939	0.640	0.948	0.747	0.902
You [5]	0.941	0.877	0.487	0.919	0.730	0.881
C. MS-SSIM [18]	0.942	0.912	0.603	0.942	0.776	0.917
Hewage [6]	0.895	0.904	0.530	0.798	0.669	0.830
SSPM	0.915	0.909	0.744	0.909	0.771	0.922
Chen [17]	0.917	0.907	0.695	0.917	0.735	0.895
Akhter [19]	0.904	0.905	0.729	0.617	0.503	0.626

TABLE III. RMSE VALUES OF THE MAINSTREAM 3D IQA METRICS ON THE LIVE 3D DATABASE PHASE 1

Algorithm	WN	JP2K	JPEG	GBlur	FF	All
Benoit [4]	6.307	4.426	5.022	4.571	8.257	7.061
You [5]	5.621	6.206	5.709	5.679	8.492	7.746
C. MS-SSIM [18]	5.581	5.320	5.216	4.822	7.837	6.533
Hewage [6]	7.405	5.530	5.543	8.748	9.226	9.139
SSPM	2.263	2.121	1.921	2.169	2.517	2.211
Chen [17]	6.433	5.402	4.523	5.898	8.322	7.247
Akhter [19]	7.092	5.483	4.273	11.387	9.332	14.827

TABLE IV. SROCC VALUES OF THE MAINSTREAM 3D IQA METRICS ON THE LIVE 3D DATABASE PHASE 2

Algorithm	WN	JP2K	JPEG	GBlur	FF	All
Benoit [4]	0.923	0.751	0.867	0.455	0.773	0.728
You [5]	0.909	0.894	0.795	0.813	0.891	0.786
C. MS-SSIM [18]	0.940	0.814	0.843	0.908	0.884	0.889
Hewage [6]	0.880	0.598	0.736	0.028	0.684	0.501
SSPM	0.940	0.751	0.768	0.900	0.920	0.820
Chen [17]	0.950	0.867	0.867	0.900	0.933	0.880
Akhter [19]	0.714	0.724	0.649	0.682	0.559	0.543

TABLE V. PLCC VALUES OF THE MAINSTREAM 3D IQA METRICS ON THE LIVE 3D DATABASE PHASE 2

Algorithm	WN	JP2K	JPEG	GBlur	FF	All
Benoit [4]	0.926	0.784	0.853	0.535	0.807	0.748
You [5]	0.912	0.905	0.830	0.784	0.915	0.800
C. MS-SSIM [18]	0.957	0.834	0.862	0.963	0.901	0.900
Hewage [6]	0.891	0.664	0.734	0.450	0.746	0.558
SSPM	0.918	0.752	0.788	0.938	0.914	0.824
Chen [17]	0.947	0.899	0.901	0.941	0.932	0.895
Akhter [19]	0.722	0.776	0.786	0.795	0.674	0.568

B. Performance on LIVE 3D Database Phase 2

Table IV-VI present the performance comparison on the LIVE 3D database Phase 2, while the scatter plots of differential MOS (DMOS) versus SSPM are shown in Fig. 7 . It can be seen that our proposed SSPM metric also has a quite advanced and competitive performance, especially as far as RMSE values are concerned, even though the distorted dataset contains both symmetric and asymmetric stimuli. Considering that our model does not work very well for some distortion types, such as JPEG2000 compression, yet we admit that there are still margins for improvement of the SSPM metric, which provides us a promising direction for future study.

IV. CONCLUSION

In this paper, we develop a Structural degradation and Saliency based Parallax compensation Model (SSPM) inspired reduced-reference stereoscopic IQA approach. This method mainly consists of the following three parts: feature extraction with structural degradation detection, saliency based parallax compensation on uncomfortable parallax, and an effective nonlinear combination. Experimental results on the LIVE 3D Image Quality Database verified that the performance of the proposed method is quite an advanced and competitive one among the mainstream NR, RR and FR stereoscopic image quality metrics. Furthermore, our IQA algorithm has a remark-

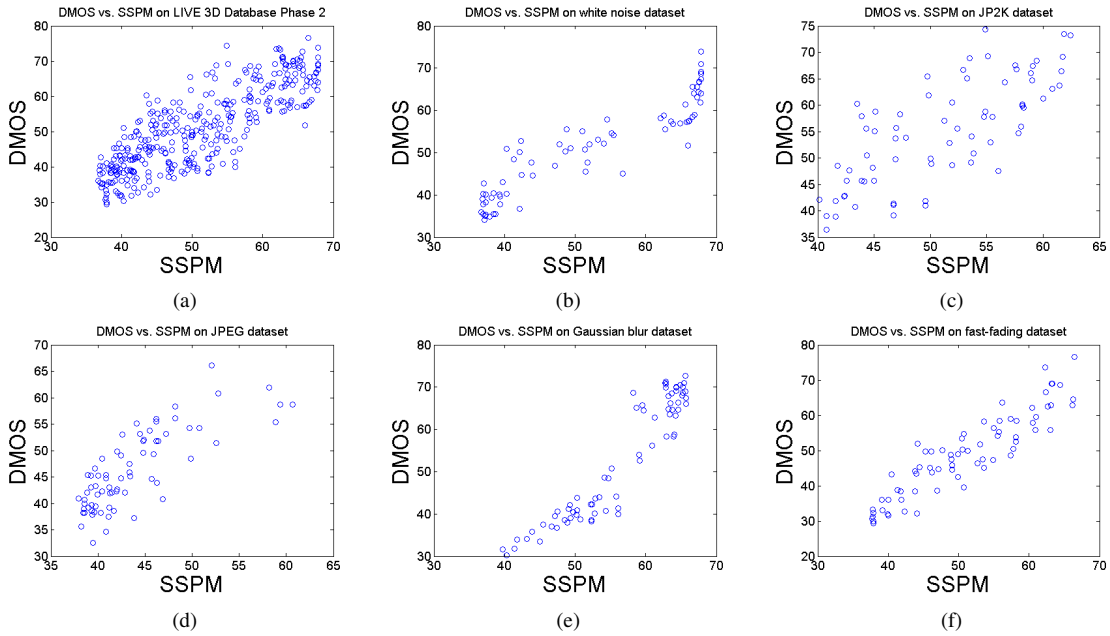

Fig. 7. Scatter plots of DMOS vs. the proposed SSPM metric on the whole LIVE 3D database Phase 2 and five data sets of different distortion types.

TABLE VI. RMSE VALUES OF THE MAINSTREAM 3D IQA METRICS ON THE LIVE 3D DATABASE PHASE 2

Algorithm	WN	JP2K	JPEG	GBlur	FF	All
Benoit [4]	4.028	6.096	3.787	11.763	6.894	7.490
You [5]	4.396	4.186	4.086	8.649	4.649	6.772
C. MS-SSIM [18]	3.368	5.562	3.865	3.747	4.966	4.987
Hewage [6]	10.713	7.343	4.976	12.436	7.667	9.364
SSPM	1.947	2.470	2.031	2.672	2.116	2.264
Chen [17]	3.513	4.298	3.342	4.725	4.180	5.102
Akhter [19]	7.416	6.189	4.535	8.450	8.505	9.294

able merit that only negligible amount of information (four number pairs) is needed to be transmitted to the receiver end, which can be easily encoded into file headers.

ACKNOWLEDGMENT

This work was supported in part by NSFC (61025005, 61371146, 61221001), 973 Program (2010CB731401) and FANEDD (201339).

REFERENCES

[1] Z. Wang, A. C. Bovik, H. R. Sheikh, and E. P. Simoncelli, *Image Quality Assessment: From Error Visibility to Structural Similarity*. IEEE Trans. Image Process., vol. 13, no. 4, pp. 600-612, April 2004.

[2] Z. Wang, E. P. Simoncelli, and A. C. Bovik, *Multi-scale Structural Similarity for Image Quality Assessment*. IEEE Asilomar Conference Signals, Systems and Computers, November 2003.

[3] H. R. Sheikh, and A. C. Bovik, *Image Information and Visual Quality*. IEEE Trans. Image Process., vol. 15, no. 2, pp. 430-444, February 2006.

[4] A. Benoit, P. Le Callet, P. Campisi, and R. Cousseau, *Quality Assessment of Stereoscopic Images*. EURASIP Journal on Image and Video Processing, vol. 2008, Article ID 659024, 2008.

[5] J. You, L. Xing, A. Perkis, and X. Wang, *Perceptual Quality Assessment for Stereoscopic Images Based On 2D Image Quality Metrics and Disparity Analysis*. Proceedings of the International Workshop on Video Processing and Quality Metrics, 2010.

[6] C. T. E. R. Hewage, and M. G. Martini, *Reduced-reference Quality Metric for 3D Depth Map Transmission*. Proc. IEEE Int. Conf. Image Process., 2010.

[7] K. Gu, G. Zhai, X. Yang, and W. Zhang, "A new no-reference stereoscopic image quality assessment based on ocular dominance theory and degree of parallax," *in Proc. IEEE Int. Conf. Pattern Recognition*, pp. 206-209, Nov. 2012.

[8] K. Gu, G. Zhai, X. Yang, and W. Zhang, "No-reference stereoscopic IQA approach: From nonlinear effect to parallax compensation", *Journal of Electrical and Computer Engineering*, vol. 2012, Article ID 436031, 2012.

[9] Z. Wang, H. R. Sheikh, and A. C. Bovik, *No-reference perceptual quality assessment of JPEG compressed images*. Proc. IEEE Int. Conf. Image Process., September 2002.

[10] Z. Wang, and A. C. Bovik, *Modern Image Quality Assessment*. Synthesis Lectures on Image, Video & Multimedia Processing, Morgan & Claypool Publishers, 2006.

[11] K. Gu, G. Zhai, X. Yang, and W. Zhang, *A New Reduced-reference Image Quality Assessment Using Structural Degradation Model*. Proc. IEEE International Symposium on Circuits and Systems, 2013.

[12] K. Gu, G. Zhai, X. Yang, and W. Zhang, *An Improved Full-reference Image Quality Metric Based On Structure Compensation*. APSIPA ASC, 2012.

[13] A. K. Moorthy, C. C. Su, A. Mittal, and A. C. Bovik, *Subjective Evaluation of Stereoscopic Image Quality*. Signal Processing: Image Communications, 2012.

[14] S. Yano, S. Ide, T. Mitsuhashi, and H. Thwaites, *A Study of Visual Fatigue and Visual Comfort for 3D HDTV/HDTV Images*. Displays, 2002.

[15] L. Itti, C. Koch, and E. Niebur, *A Model of Saliency Based Visual Attention for Rapid Scene Analysis*. IEEE Transaction on Pattern Analysis and Machine Intelligence, vol. 20, pp. 1254-1259, 1998.

[16] VQEG, *Final Report from The Video Quality Experts Group on The Validation of Objective Models of Video Quality Assessment*. March 2000, http://www.vqeg.org/.

[17] M. Chen, L. K. Cormack, and A. C. Bovik, *No-Reference Quality Assessment of Natural Stereopairs*. IEEE Transaction on Image Processing, Vol. 22, No. 9, September 2013.

[18] M. Chen, C. Su, D. Kwon, L. K. Cormack and A. C. Bovik, *Full-reference quality assessment of stereopairs accounting for rivalry*. Signal Processing: Image Communication, 2013.

[19] R. Akhter, J. Baltes, Z. M. Parvez Sazzad, and Y. Horita, *No-reference stereoscopic image quality assessment.* Proc. SPIE, vol. 7524, p. 75240T, Feb. 2010.